RSC Advances

PAPER

Cite this: *RSC Adv.*, 2015, **5**, 84643

Synthesis, linear and nonlinear optical properties of thermally stable ferrocene-diketopyrrolopyrrole dyads†

Sarbjeet Kaur,[a] Sugandha Dhoun,[a] Griet Depotter,[b] Paramjit Kaur,*[a] Koen Clays[b] and Kamaljit Singh*[a]

Received 4th September 2015
Accepted 29th September 2015

DOI: 10.1039/c5ra17977g

www.rsc.org/advances

A set of new ferrocene-diketopyrrolopyrrole (Fc-DPP) conjugated dyads was synthesized and their optical, nonlinear optical (NLO) and electrochemical properties were investigated. The second-order nonlinear polarizabilities were determined using hyper-Rayleigh scattering with femtosecond pulsed laser light at 840 nm. The dyads exhibited structure dependent NLO response, which could be explained by correlating optical as well as electrochemical data. In the latter case, it is shown that the amplitude of the Fc based one-electron redox process of D–π–A type dyads is doubled in the dyads of the type D–π–A–π–D, where the acceptor (DPP) is flanked by two Fc donors.

Introduction

Materials exhibiting nonlinear optical (NLO)[1–5] response are of great interest for the development of optical devices for applications in the field of photonics,[6,7] nanophotonics[8] and optoelectronics[9–12] such as optical signal processing, broad band optical communications, integrated optics, optical sensing, optical poling, optical limiting, optical computing *etc.* Standard materials generally contain a donor–acceptor combination linked by a conjugated bridge.[13–15] The NLO response of ferrocene (Fc) based dyads has been a subject of numerous investigations owing to many attractive features of this organometallic species.[16–18] Depending upon the oxidation state of the metal centre, the Fc unit can turn a strong donor or acceptor, a feature that has also been exploited in the reversible redox switching of the NLO response in Fc dyads.[19–24] Ferrocene dyads generally possess low oxidation potential and upon facile charge transfer (CT) to an acceptor yield stable α-ferrocenyl carbocations.[17,25,26] Further, as a specific feature of the substitution pattern of the Fc unit, the non-centrosymmetric dyads are associated with high optical nonlinearities.[22,27–29] Suitably functionalized push–pull dyads (D–π–A) in which electron donor (D) Fc is connected by π-conjugating spacers to strong electron acceptors (A), have witnessed significant interest in their synthesis, owing to their structure dependent electrochemical, optical and nonlinear optical properties.[28,30,31] Correlating the absorption, electrochemical, theoretical calculations and Hyper-Rayleigh Scattering (HRS) experiments, we earlier[23] demonstrated that varying the conjugation pathway between D (Fc) and A (increasing π-bridge length) has more impact (greater red shift of the absorption band and smaller optical band gap) on the NLO response than by modulating the acceptor strength.[23] As a consequence, the Fc based (D–π–A) compounds with shortest conjugation path showed higher intrinsic hyperpolarizability. Additionally, owing to their reversible redox behaviour, these chromophores recorded different hyperpolarizability values in each of the two redox states and a high on/off (β_{on}/β_{off}) ratio. Among the various known acceptors such as thiazole,[32] and benzodiazthiazole,[33] diketopyrrolopyrrole unit[34–36] has emerged a promising candidate for optoelectronics[37] and organic photovoltaics[34,38] such as organic light emitting diodes (OLEDs),[39–41] organic field effect transistors (OFETs),[42–44] organic solar cells (OSCs),[45–47] dye sensitized solar cells (DSSCs)[48,49] *etc.* This sub-unit has two amide groups that make it a strong acceptor, and consequently the energy of the lowest unoccupied molecular orbital (LUMO) of D–A or D–π–A systems, wherein appropriately substituted diketopyrrolopyrrole is used as acceptor, is considerably lowered.[50] In addition to a good acceptor, this planar, conjugated bicyclic core[51] also possesses exceptionally high photochemical, mechanical and thermal stability,[34] thus rendering it a good candidate for π-conjugated donor–acceptor (D–A) dyads. To the best of our knowledge, the second-order nonlinear polarizability (β) of diketopyrrolopyrrole-based dyads has not been explored yet.

In this work, new dyads having a Fc donor and an appropriately substituted 2,5-bis-(*n*-decyl)-3,6-di(furan-2-yl)pyrrolo[3,4-*c*]-pyrrole-1,4(2*H*,5*H*)-dione (DPP) acceptor,[50,52–55] intercepted by a conjugated linker (Fig. 1A and B), representing D–A or D–A–D type design in which the acceptor is flanked by two Fc units

[a]*Department of Chemistry, UGC-Centre of Advance Study-II, Guru Nanak Dev University, Amritsar-143005, India. E-mail: kamaljit.chem@gndu.ac.in*

[b]*Department of Chemistry, University of Leuven, Celestijnenlaan 200D, B-3001 Leuven, Belgium. E-mail: Koen.Clays@fys.kuleuven.be*

† Electronic supplementary information (ESI) available. See DOI: 10.1039/c5ra17977g

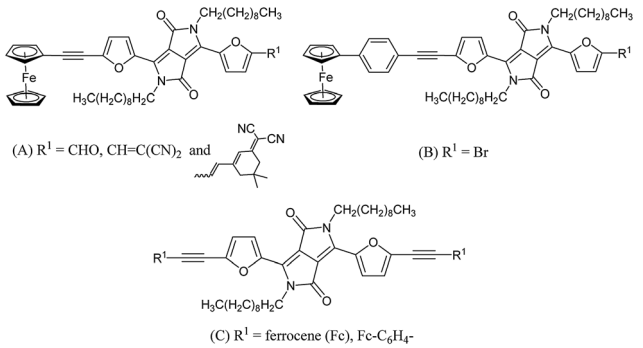

Fig. 1 Chemical structures of Fc-DPP dyads: D–A (A and B), D–A–D (C).

through a conjugated bridge (Fig. 1C) have been prepared. Their structure is determined by means of microanalytical data, ^{1}H and ^{13}C NMR, UV-visible, and FTIR spectroscopy. The NLO properties have been determined in THF solution by means of the HRS technique (under femtosecond pulsed 840 nm laser light). The experimental linear optical properties of the above derivatives have also been computed by employing density functional theory (DFT) calculations and revealed a good correlation between the experimental results and the theoretically calculated data. Energies of the frontier molecular orbitals (FMOs) have been computed from time dependent DFT calculations and spectral resolution has been achieved by band fitting. Moreover, the structure-polarization (dipole moment) relationship has been analysed and the effect of the molecular design on the observed linear, electrochemical and NLO properties has been discussed.

Experimental section

Materials and reagents

All liquid reagents were dried/purified by using the recommended drying agents and/or distilled over 4 Å molecular sieves. Tetrahydrofuran was dried using sodium metal/benzophenone, while chloroform and dichloromethane were dried over fused $CaCl_2$. Triethylamine and piperidine were distilled and stored over KOH under nitrogen. *N*,*N*-Dimethylformamide was distilled over CaH_2 and stored over 4 Å molecular sieves. Acetyl ferrocene **6a**,[56] 2-(3,5,5-trimethyl-2-cyclohexenylidene)malononitrile **10** [57] and bistriphenylphosphinedichloropalladium(II)[58] were prepared following the reported procedures. Ferrocene, phosphorous oxychloride, 1-bromodecane, bromine, 4-aminoacetophenone and malononitrile were purchased from Spectrochem and used as received. K_2CO_3 was dried at 120 °C overnight in a furnace. 2-Furonitrile, 2-methyl-1-butanol and copper(I) iodide were purchased from Sigma-Aldrich and used as such.

Instrumentation

UV-visible studies were carried out using HITACHI U-2910 Spectrophotometer. ^{1}H NMR and ^{13}C NMR spectra were recorded on Bruker Biospin Avance III HD at 500 MHz, in $CDCl_3$ and/or DMSO-d_6 containing TMS as internal standard. Data are reported as follows: chemical shift in ppm (δ), integration, multiplicity (s = singlet, d = doublet, t = triplet, m = multiplet, br = broad) and coupling constant J (Hz). The purity of the compounds was determined by elemental analysis carried out on Thermoscientific FLASH 2000 organic elemental analyzer and was within ±0.4% of the theoretical values. IR spectrum was recorded on Perkin-Elmer FTIR-C92035 Fourier-transform spectrophotometer in range 400–4000 cm^{-1} as KBr pellets. All reported yields are isolated yields. Melting points were recorded in open capillaries and are uncorrected. For column chromatography, silica gel (60–120 mesh) and/or neutral alumina were employed and eluted with ethyl acetate/hexane or chloroform/hexane mixtures. Electrochemical measurements were made using CHI660D electrochemical workstation using three electrodes-platinum as working as well as counter electrode and Ag/AgCl as reference electrode. The experiments were carried at 1×10^{-4} M solution of the compound in dichloromethane using 2×10^{-2} M tetrabutylammoniumhexafluorophosphate as supporting electrolyte. The solutions were purged with nitrogen for 10 min and the working electrode as well as the reference electrode was cleaned after each reading. The experiments were carried out at scan rate of 100 mV s^{-1}. Thermogravimetric analysis were recorded on TGA/DSC 1 STAR System from Mettler Toledo in the temperature range of 0–800 °C at the heating rate of 10 °C min^{-1} under nitrogen atmosphere. Femtosecond HRS measurements[59–64] were performed at 840 nm using a commercial Ti : sapphire laser at ambient temperature. Crystal violet in methanol was used as the reference, with a value of 434×10^{-30} esu at 840 nm for the octopolar β_{xxx} hyperpolarizability tensor component.

Computational details

Theoretical calculations were carried out by using the Gaussian 09 suite of programs.[65] Optimization of molecular geometries of all the chromophores and related calculations were performed by density functional theory (DFT) method using B3LYP functional group and 6-31G as the basis set. The first 15–30 excited states were calculated by using time-dependent density functional theory (TD-DFT calculations) in gas phase as well in dichloromethane as solvent using CPCM model. The molecular orbital contours were plotted using Gauss view 5.0.9.

Synthesis of dyads and intermediates

Synthesis of 3,6-di(furan-2-yl)pyrrolo[3,4-*c*]pyrrole-1,4-(2*H*,5*H*)-dione 1. Nitrogen was purged (15 min) in 2-methyl-1-butanol (60 ml) contained in a three-neck round bottomed flask (250 ml) equipped with a reflux condenser. Sodium metal (3.45 g, 150 mmol) and $FeCl_3$ (0.05 g, 0.31 mmol) were added and the reaction mixture was heated at 90 °C until sodium metal had completely reacted (indicated by complete dissolution). The reaction mixture was cooled to 85 °C and 2-furonitrile (9.31 g, 100 mmol) was added followed by dropwise addition of diisopropyl succinate (8.10 g, 40 mmol) over a period of 1 h. Reaction mixture was heated at 85 °C for 2 h, after which it was cooled to 50 °C and 50 ml methanol was added. The reaction

mixture was neutralized using glacial acetic acid and stirred for 15 min and then cooled to ambient temperature and the contents were filtered over sintered glass (G4) funnel. Residue was washed twice with hot methanol and de-ionized water to yield analytically pure dark red solid **1** (61%). Mp > 300 °C IR (KBr): ν_{max} 1628, 1648, 3153 and 3417 cm^{-1}. ^1H (500 MHz, DMSO-d_6, 25 °C): δ (ppm) 5.97 (s, 2H, furanyl C4–CH), 6.79 (s, 2H, furanyl C3–CH), 7.18 (s, 2H, furanyl C2–CH) and 10.33 (br, 2H, –NH). ^{13}C NMR (125 MHz, $CDCl_3$, 25 °C): δ (ppm) 108.05, 114.15, 117.24, 131.74, 144.22, 147.33 and 161.63. Anal. calcd for $C_{14}H_8N_2O_4$: C, 62.69; H, 3.01; N, 10.44. Found: C, 62.73; H, 3.00; N, 10.48.

Synthesis of 2,5-bis-(*n*-decyl)-3,6-di(furan-2-yl)pyrrolo-[3,4-*c*]-pyrrole-1,4-(2*H*,5*H*)-dione 2. To a solution of **1** (3 g, 11.2 mmol) in anhydrous DMF (250 ml) under blanket of anhydrous N_2 gas, anhydrous K_2CO_3 (4.64 g, 33.60 mmol) was added and the reaction mixture was heated at 120 °C for 1 h. 1-Bromodecane (7.44 g, 33.60 mmol) was added dropwise and reaction was stirred for 12 h at 120 °C until it completed. DMF was removed under reduced pressure and the residue was extracted with chloroform (3 × 30 ml). The extract was washed twice with water and the dried (over anhydrous sodium sulphate) organic layer was evaporated under reduced pressure to obtain crude **2**, which was purified by column chromatography using 5 : 95 (ethyl acetate/hexane) as eluent to obtain dark red solid **2** (48%). Mp 80–82 °C IR (KBr): ν_{max} 1590, 1669, 2850, 2917, 2955, 3106 and 3155 cm^{-1}. ^1H (500 MHz, $CDCl_3$, 25 °C): δ (ppm) 0.87 (t, J = 5 Hz, 6H, $-CH_3$), 1.25–1.40 (m, 28H, $-CH_2$), 1.66–1.72 (m, 4H, $-CH_2$), 4.04–4.12 (m, 4H, $-CH_2$), 6.69–6.70 (dd, 2H, furanyl C3–CH), 7.63 (d, J = 5 Hz, 2H, furanyl C4–CH) and 8.30 (d, J = 5 Hz, 2H, furanyl C2–CH). ^{13}C NMR (125 MHz, $CDCl_3$, 25 °C): δ (ppm) 14.10, 22.68, 25.97, 26.86, 29.12, 29.31, 29.55, 30.22, 31.90, 42.43, 106.48, 113.45, 120.08, 133.67, 144.70, 145.13 and 160.88. Anal. calcd for $C_{34}H_{48}N_2O_4$: C, 74.42; H, 8.82; N, 5.10. Found: C, 74.52; H, 8.86; N, 5.09.

Synthesis of 3,6-bis-(5-bromofuran-2-yl)-2,5-bis-(*n*-decyl)-pyrrolo[3,4-*c*]pyrrole-1,4-(2*H*,5*H*)-dione 3. A solution of bromine (1.93 g, 12.10 mmol) in $CHCl_3$ (100 ml) was slowly added to a solution of **2** (3 g, 5.50 mmol) anhydrous $CHCl_3$ (150 ml) precooled to 0 °C. The reaction mixture was stirred for completion at the same low temperature and treated with saturated aqueous solution of sodium thiosulphate. The bromine free solution was extracted with chloroform (3 × 30 ml) and the organic extract was washed with water (2 × 25 ml). The organic extract was dried over anhydrous sodium sulphate, filtered and evaporated under reduced pressure to obtain crude **3**, which was purified by column chromatography using 30 : 70 ($CHCl_3$/hexane) as eluents to obtain dark red solid **3** (58%). Mp 138–140 °C IR (KBr): ν_{max} 1548, 1584, 1665, 2851, 2919, 2954 and 3128 cm^{-1}. ^1H (500 MHz, $CDCl_3$, 25 °C): δ (ppm) 0.87 (t, J = 7.5 Hz, 6H, $-CH_3$), 1.26–1.42 (m, 28H, $-CH_2$), 1.66–1.72 (m, 4H, $-CH_2$), 4.06 (t, J = 7.5 Hz, 4H, $-CH_2$), 6.62 (d, J = 5 Hz, 2H, furanyl C3–CH) and 8.25 (d, J = 5 Hz, 2H, furanyl C4–CH). ^{13}C NMR (125 MHz, $CDCl_3$, 25 °C): δ (ppm) 14.13, 22.69, 26.86, 29.28, 29.30, 29.53, 29.59, 30.20, 31.90, 42.50, 106.28, 115.51, 122.10, 126.41, 132.51, 146.17 and 160.52. Anal. calcd for $C_{34}H_{46}Br_2N_2O_4$: C, 57.80; H, 6.56; N, 3.96. Found: C, 57.89; H, 6.59; N, 3.95.

Synthesis of 5-(2,5-bis-(*n*-decyl)-4-(furan-2-yl)-3,6-dioxo-2,3,5,6-tetrahydropyrrolo[3,4-*c*]pyrrol-1-yl)furan-2-carbaldehyde 4. Vilsmeier–Haack formylation of **2** was performed by mixing anhydrous DMF (10 ml) and $POCl_3$ (0.38 g, 2.48 mmol) and stirring the solution at 0 °C for 1 h to provide the red coloured chloroiminium ion (Vilsmeier reagent). Solution of **2** (0.5 g, 0.91 mmol) in anhydrous DMF (5 ml) was added to this reagent at 0 °C and the reaction warmed and stirred at 100 °C for 4 h. Subsequent to the completion (TLC), the reaction mixture was cooled and quenched with pre-cooled saturated aqueous solution of sodium acetate and extracted with DCM (3 × 30 ml). The organic extract was washed with water (2 × 25 ml), dried over anhydrous sodium sulfate and evaporated under reduced pressure to obtain crude **4**, which was purified by column chromatography using 5 : 95 (ethyl acetate/hexane) as eluents to obtain dark red solid **4** (50%). Mp 80–82 °C IR (KBr): ν_{max} 1587, 1668, 2850, 2919 and 3124 cm^{-1}. ^1H (500 MHz, $CDCl_3$, 25 °C): δ (ppm) 0.87 (t, J = 7.5 Hz, 6H, $-CH_3$), 1.25–1.43 (m, 28H, $-CH_2$), 1.68–1.74 (m, 4H, $-CH_2$), 4.10–4.19 (m, 4H, $-CH_2$), 6.74–6.75 (dd, 1H, furanyl C3′–CH), 7.41 (d, J = 5 Hz, 1H, furanyl C4′–CH), 7.70 (d, J = 1.5 Hz, 1H, furanyl C2′–CH), 8.34 (d, J = 4 Hz, 1H, furanyl C4–CH), 8.47 (d, J = 5 Hz, 1H, furanyl C3–CH) and 9.74 (s, 1H, CHO). ^{13}C NMR (125 MHz, $CDCl_3$, 25 °C): δ (ppm) 14.12, 22.69, 29.30, 29.35, 29.52, 29.58, 29.62, 29.65, 31.88, 31.92, 42.77, 106.78, 110.56, 113.90, 119.86, 122.26, 144.30, 146.28, 148.32, 152.77, 160.33, 161.10 and 177.00. Anal. calcd for $C_{35}H_{48}N_2O_5$: C, 69.65; H, 6.68; N, 6.63. Found: C, 69.73; H, 6.70; N, 6.66.

Synthesis of 5-(4-(5-bromofuran-2-yl)-2,5-bis-(*n*-decyl)-3,6-dioxo-2,3,5,6-tetrahydropyrrolo[3,4-*c*]pyrrol-1-yl)furan-2-carbaldehyde 5. A solution of **4** (0.13 g, 0.23 mmol) in anhydrous $CHCl_3$ (15 ml) was cooled to 0 °C and portion-wise addition of NBS (0.043 g, 0.24 mmol) was made and the reaction mixture stirred at 0 °C for 2 h. After completion of the reaction (TLC), saturated aqueous solution of sodium thiosulfate was introduced to quench the reaction and extracted with chloroform (3 × 25 ml). The extract was washed with water (2 × 20 ml), dried over anhydrous sodium sulfate and evaporated under reduced pressure to obtain crude **5**, which was recrystallized from hexane to obtain dark red solid **5** (71%). Mp 140–142 °C IR (KBr): ν_{max} 1584, 1666, 2850, 2920 and 3128 cm^{-1}. ^1H (500 MHz, $CDCl_3$, 25 °C): δ (ppm) 0.87 (t, J = 7.5 Hz, 6H, $-CH_3$), 1.24–1.44 (m, 28H, $-CH_2$), 1.69–1.74 (m, 4H, $-CH_2$), 4.06–4.18 (m, 4H, $-CH_2$), 6.67 (d, J = 5 Hz, 1H, furanyl C4′–CH), 7.41 (d, J = 5 Hz, 1H, furanyl C3′–CH), 8.34 (d, J = 5 Hz, 1H, furanyl C4–CH), 8.40 (d, J = 5 Hz, 1H, furanyl C3–CH) and 9.74 (s, 1H, –CHO). ^{13}C NMR (125 MHz, $CDCl_3$, 25 °C): δ (ppm) 14.12, 22.68, 26.85, 29.26, 29.30, 29.53, 30.16, 30.39, 31.89, 42.63, 42.82, 106.52, 115.92, 120.11, 123.87, 127.76, 134.35, 145.84, 148.15, 152.85, 160.23, 160.87 and 177.03. Anal. calcd for $C_{35}H_{47}BrN_2O_5$: C, 64.11; H, 7.23; N, 4.27. Found: C, 63.88; H, 6.96; N, 4.43.

Synthesis of 4-ferrocenylethynylbenzene 6b. A solution of sodium nitrite (30.36 g, 44.00 mmol) in 20 ml water precooled to 0 °C was added dropwise to a stirred solution of 4-amino-acetophenone (3 g, 22.00 mmol) in 2 : 1 THF/hydrochloric acid (24 ml) kept at 0 °C and the mixture was stirred at 0 °C for 30 min to ensure complete diazotization. Separately, ferrocene

(6.95 g, 37.40 mmol) was added to 48 ml sulphuric acid and the resulting deep blue solution of ferrocenium ion was stirred at ambient temperature for 2 h. The solution of the ferrocenium ion was then poured in crushed ice and warmed to room temperature after which addition of copper powder (1.82 g) was made. Addition of the diazonium salt solution prepared as above was made dropwise and the reaction mixture stirred for 24 h at room temperature. Ascorbic acid (9.11 g, 51.72 mmol) was added to reduce the unreacted ferrocenium ion to ferrocene. Reaction mixture was passed through celite and the filtrate was extracted with DCM (3 × 30 ml). The DCM extract was then washed with water (2 × 25 ml), dried over anhydrous sodium sulfate and the solvent removed under vacuum to obtain crude **6b**, which was purified by column chromatography using 10 : 90 (ethyl acetate/hexane) as eluents to isolate pure **6b** as orange solid (40%). Mp 156–158 °C (hexane) IR (KBr): ν_{max} 1030, 1415, 1563, 1602, 1669, 2956, 2997, 3079 and 3104 cm^{-1}. ^1H (500 MHz, $CDCl_3$, 25 °C): δ (ppm) 2.60 (s, 3H, $-CH_3$), 4.04 (s, 5H, Fc), 4.41 (s, 2H, Fc), 4.72 (s, 2H, Fc), 7.53 (d, $J = 10$ Hz, 2H, $-C_6H_5$) and 7.88 (d, $J = 10$ Hz, 2H, $-C_6H_5$). ^{13}C NMR (125 MHz, $CDCl_3$, 25 °C): δ (ppm) 26.49, 66.94, 69.85, 69.89, 125.76, 128.60, 134.62, 145.52 and 197.54. Anal. calcd for $C_{18}H_{16}FeO$: C, 71.08; H, 5.30. Found: C, 71.12; H, 5.32.

General procedure for synthesis of 7a,b. Vilsmeier–Haack formylation of **6a** and **6b** (50 mmol) was performed by mixing anhydrous DMF (192 mmol) and $POCl_3$ (192 mmol) and stirring the solution at 0 °C for 1 h to provide the red coloured chloroiminium ion (Vilsmeier reagent). Solution of appropriate **6** (50 mmol) in anhydrous DMF (30 ml) was added to this reagent at 0 °C and stirred at 0 °C for 4 h. Subsequent to the completion (TLC), the reaction mixture was cooled and quenched with precooled saturated aqueous solution of sodium acetate and extracted with ether (3 × 30 ml). The organic extract was washed with water (2 × 25 ml), dried over anhydrous sodium sulfate and evaporated under reduced pressure to obtain analytically pure solid **7**.

*(2-Formyl-1-chlorovinyl)ferrocene **7a**.* Red solid, yield: 90%. Mp 72–74 °C IR (KBr): ν_{max} 1029, 1417, 1617, 2849, 2924 and 2956 cm^{-1}. ^1H (500 MHz, $CDCl_3$, 25 °C): δ (ppm) 4.25 (s, 5H, Fc), 4.57 (s, 2H, Fc), 4.75 (s, 2H, Fc), 6.41 (s, 1H, –CH) and 10.10 (s, 1H, CHO). ^{13}C NMR (125 MHz, $CDCl_3$, 25 °C): δ (ppm) 68.91, 70.84, 72.31, 120.48, 155.29 and 190.82. Anal. calcd for $C_{13}H_{11}ClFeO$: C, 56.88; H, 4.04. Found: C, 56.93; H, 4.03.

*(4-(2-Formyl-1-chlorovinyl)phenyl]ferrocene **7b**.* Red solid, yield: 97%. Mp 100–102 °C IR (KBr): ν_{max} 1032, 1591, 1668, 2860, 2921, 3085 and 3100 cm^{-1}. ^1H (500 MHz, $CDCl_3$, 25 °C): δ (ppm) 4.05 (s, 5H, Fc), 4.42 (s, 2H, Fc), 4.72 (s, 2H, Fc), 6.71 (d, $J = 10$ Hz, 1H, –CH), 7.53 (d, $J = 10$ Hz, 2H, $-C_6H_5$), 7.69 (d, $J = 5$ Hz, 2H, $-C_6H_5$) and 10.23 (d, $J = 5$ Hz, 1H, –CHO). ^{13}C NMR (125 MHz, $CDCl_3$, 25 °C): δ (ppm) 66.87, 69.89, 69.99, 82.97, 123.14, 126.07, 127.33, 132.40, 144.66 and 191.57. Anal. calcd for $C_{19}H_{15}ClFeO$: C, 65.09; H, 4.31. Found: C, 65.04, H, 4.33.

General procedure for synthesis of 8a,b. A solution of appropriate **7a**/**7b** (47.50 mmol) in dioxane (150 ml) was heated at 110 °C for 15 min and 1 N NaOH (125 ml) was added and reaction mixture was stirred at the same temperature for 1 h. The contents of the reaction were poured into ice, neutralized with 1 N HCl, passed through Celite. The filtrate was extracted with hexane (3 × 30 ml). The hexane extract was dried over anhydrous sodium sulfate and the solvent removed under reduced pressure to obtain corresponding crude **8a**/**8b**, respectively, which was purified by column chromatography using hexane as eluents to isolate pure **8a**/**8b**, respectively.

*Ethynylferrocene **8a**.* Orange solid, yield: 72%. Mp 50–52 °C (hexane) IR (KBr): ν_{max} 1022, 1443, 1639, 2104, 2854, 2924, 3089, 3105 and 3280 cm^{-1}. ^1H (500 MHz, $CDCl_3$, 25 °C): δ (ppm) 2.72 (s, 1H, –CH), 4.19 (s, 2H, Fc), 4.21 (s, 5H, Fc) and 4.45 (s, 2H, Fc). ^{13}C NMR (125 MHz, $CDCl_3$, 25 °C): δ (ppm) 63.87, 68.74, 70.07, 71.77 and 73.57. Anal. calcd for $C_{12}H_{10}Fe$: C, 68.62; H, 4.80. Found: C, 68.66; H, 4.82.

*(4-Ethynylphenyl)ferrocene **8b**.* Orange solid, yield: 65%. Mp 68–70 °C (hexane) IR (KBr): ν_{max} 1027, 1435, 1523, 1604, 1667, 2104, 2924, 3088 and 3286 cm^{-1}. ^1H (500 MHz, $CDCl_3$, 25 °C): δ (ppm) 3.10 (s, 1H, –CH), 4.00 (s, 5H, Fc), 4.35 (s, 2H, Fc), 4.65 (s, 2H, Fc), 7.44–7.56 (m, 4H, $-C_6H_5$). ^{13}C NMR (125 MHz, $CDCl_3$, 25 °C): δ (ppm) 66.56, 69.39, 69.72, 84.01, 84.09, 125.77, 126.38, 132.15 and 140.47. Anal. calcd for $C_{18}H_{14}Fe$: C, 75.55; H, 4.93. Found: C, 75.54; H, 4.91.

General procedure for synthesis of 9a, 9d, 9e and 9f. For the synthesis of **9a**, anhydrous nitrogen gas was filled in a septum capped three-neck round bottom flask containing **5** (0.1 g, 0.2 mmol), CuI (0.006 g, 0.02 mmol) and bistriphenylphosphinedichloropalladium(II) (0.02 g, 0.02 mmol). A mixture of THF : Et_3N (1 : 1, v/v) (10 ml) was added using hypodermic syringe and the reaction was cooled to 0 °C, followed by evacuation and refilling with N_2 gas. A solution of **8a** (0.105 g, 0.80 mmol) in anhydrous THF (5 ml) maintained under inert atmosphere was added dropwise to the reaction mixture at 0 °C using cannula and the reaction stirred at ambient temperature. After completion (TLC), the reaction mixture was passed through celite and the bed washed with DCM (20 ml). The combined filtrate was washed with water (2 × 20 ml) and the organic layer dried over anhydrous sodium sulfate and the solvent removed under reduced pressure to obtain crude **9a**, which was purified by column chromatography using 5 : 95 (ethyl acetate/hexane) as eluents to isolate analytically pure **9a**.

Following the above procedure and using **3** (0.01 g, 0. 14 mmol), CuI (0.001 g, 0.008 mmol) and bistriphenylphosphinedichloropalladium(II) (0.0089 g, 0.01 mmol) and **8a** (0.0949 g, 0.42 mmol), **9e** was obtained. Similarly, using **3** (0.1 g, 0. 14 mmol), CuI (0.001 g, 0.008 mmol) and bistriphenylphosphinedichloropalladium(II) (0.008 g, 0.01 mmol) and **8b** (0.06 g, 0.21 mmol), **9d** and **9f** were isolated in 51% and 17% yields, respectively. However, when the molar ratio of the reactants was changed to **3** (0.1 g, 0. 14 mmol), CuI (0.001 g, 0.008 mmol) and bistriphenylphosphinedichloropalladium(II) (0.008 g, 0.01 mmol) and **8b** (0.12 g, 0.42 mmol), **9d** and **9f** were isolated in 20% and 40% yields, respectively. Further, in these reactions varying but significant amounts of the corresponding diacetylene product as a consequence of Glaser coupling reaction were isolated.

*5-(2,5-Bis-(n-decyl)-3,6-dioxo-4-(5-(ferrocenylethynyl)furan-2-yl)-2,3,5,6-tetrahydropyrrolo[3,4-c]pyrrol-1-yl)furan-2-carbaldehyde **9a**.* Yield: 45%. Mp 78–80 °C (5 : 95, ethyl acetate/hexane) IR (KBr): ν_{max} 1021, 1583, 1663, 2197, 2852, 2923, 2958 and 3127 cm^{-1}.^1H

(500 MHz, $CDCl_3$, 25 °C): δ (ppm) 0.86 (t, J = 5 Hz, 6H, $-CH_3$), 1.25–1.45 (m, 28H, $-CH_2$), 1.71–1.75 (m, 4H, $-CH_2$), 4.14–4.19 (m, 4H, $-CH_2$), 4.28 (s, 5H, Fc), 4.35 (s, 2H, Fc), 4.57 (s, 2H, Fc), 6.84 (d, J = 5 Hz, 1H, furanyl C4–CH), 7.41 (d, J = 5 Hz, 1H, furanyl C3–CH), 8.35 (d, J = 4 Hz, 1H, furanyl C4′–CH), 8.50 (d, J = 5 Hz, 1H, furanyl C3′–CH) and 9.74 (s, 1H, –CHO). ^{13}C NMR (125 MHz, $CDCl_3$, 25 °C): δ (ppm) 14.13, 22.68, 26.88, 26.93, 29.30, 29.35, 29.53, 29.67, 31.88, 42.81, 62.61, 69.84, 70.30, 71.85, 98.06, 107.22, 110.88, 117.91, 119.86, 123.69, 130.75, 134.66, 141.28, 143.69, 148.40, 152.76, 160.23, 161.10 and 177.00. Anal. calcd for $C_{47}H_{56}FeN_2O_5$: C, 71.93; H, 7.19; N; 3.57. Found: C, 71.98; H, 7.22; N, 3.56.

3-(5-Bromofuran-2-yl)-6-(5-((4-ferrocenylphenyl)ethynyl)furan-2-yl)-2,5-bis-(n-decyl)-2,5-dihydropyrrolo[3,4-c]pyrrole-1,4-dione ***9d***. Yield: 51%. Mp 130–132 °C (50 : 50, $CHCl_3$/hexane) IR (KBr): ν_{max} 1026, 1550, 1580, 1668, 2192, 2851, 2922 and 2953 cm^{-1}. ^{1}H (500 MHz, $CDCl_3$, 25 °C): δ (ppm) 0.86 (t, J = 10 Hz, 6H, $-CH_3$), 1.25–1.64 (m, 28H, $-CH_2$), 1.69–1.76 (m, 4H, $-CH_2$), 4.06 (s, 5H, Fc), 4.07–4.16 (m, 4H), 4.38 (s, 2H, Fc), 4.68 (s, 2H, Fc), 6.63 (d, J = 3.5 Hz, 1H, furanyl C4′–CH), 6.88 (d, J = 5 Hz, 1H, furanyl C3′–CH), 7.44–7.48 (m, 4H, $-C_6H_5$), 8.26 (d, J = 5 Hz, 1H, furanyl C4–CH) and 8.36 (d, J = 5 Hz, 1H, furanyl C3–CH). ^{13}C NMR (125 MHz, $CDCl_3$, 25 °C): δ (ppm) 14.13, 15.00, 22.70, 26.88, 29.28, 29.37, 29.54, 29.69, 31.89, 31.91, 42.51, 48.38, 66.62, 69.65, 69.78, 83.71, 97.43, 106.70, 107.04, 115.51, 118.31, 118.45, 121.62, 122.01, 125.91, 126.31, 131.64, 132.16, 132.76, 139.87, 141.47, 144.56, 146.24, 160.53 and 160.68. Anal. calcd for $C_{52}H_{59}BrFeN_2O_4$: C, 68.50; H, 6.52; N, 3.07. Found: C, 68.53; H, 6.54; N, 3.06.

2,5-Bis-(n-decyl)-3,6-bis-(5-(ferrocenylethynyl)furan-2-yl)pyrrolo-[3,4-c]pyrrole-1,4-(2H,5H)-dione ***9e***. Dark blue solid, yield: 40%. Mp 146–148 °C (30 : 70, $CHCl_3$/hexane) IR (KBr): ν_{max} 1026, 1583, 1656, 2195, 2852, 2921 and 2953 cm^{-1}. ^{1}H (500 MHz, $CDCl_3$, 25 °C): δ (ppm) 0.86 (t, J = 5 Hz, 6H, $-CH_3$), 1.23–1.45 (m, 28H, $-CH_2$), 1.72–1.78 (m, 4H, $-CH_2$), 4.15 (t, J = 7.5 Hz, 4H, $-CH_2$), 4.27 (s, 10H, Fc), 4.33 (s, 4H, Fc), 4.56 (s, 4H, Fc), 6.81 (d, J = 5 Hz, 2H, furanyl C4–CH) and 8.35 (d, J = 5 Hz, 2H, furanyl C3–CH). ^{13}C NMR (125 MHz, $CDCl_3$, 25 °C): δ (ppm) 14.13, 22.69, 26.97, 29.36, 29.57, 29.68, 29.70, 30.29, 31.89, 42.59, 62.92, 69.67, 70.25, 71.77, 97.04, 107.23, 117.71, 121.55, 132.35, 140.13, 144.21 and 160.74. Anal. calcd for $C_{58}H_{64}Fe_2N_2O_4$: C, 72.20; H, 6.69; N, 2.90. Found: C, 72.26; H, 6.66; N, 2.89.

3,6-bis(5-((4-ferrocenyl)phenylethynyl)furan-2-yl)-2,5-bis-(n-decyl)-pyrrolo[3,4-c]pyrrole-1,4-(2H,5H)-dione ***9f***. Dark blue solid, yield: 40%. Mp 140–142 °C (40 : 60, $CHCl_3$/hexane) IR (KBr): ν_{max} 1031, 1553, 1579, 2192, 2852, 2920 and 3094 cm^{-1}. ^{1}H (500 MHz, $CDCl_3$, 25 °C): δ (ppm) 0.87 (t, J = 7.5 Hz, 6H, $-CH_3$), 1.25–1.47 (m, 28H, $-CH_2$), 1.74–1.80 (m, 4H, $-CH_2$), 4.06 (s, 10H, Fc), 4.17 (t, J = 7.5 Hz, 4H), 4.39 (s, 4H, Fc), 4.68 (s, 4H, Fc), 6.89 (d, J = 5 Hz, 2H, furanyl C4–CH), 7.45–7.49 (m, 8H, $-C_6H_5$), and 8.39 (d, J = 4 Hz, 2H, furanyl C3–CH). ^{13}C NMR (125 MHz, $CDCl_3$, 25 °C): δ (ppm) 14.11, 22.70, 25.97, 28.98, 29.12, 29.17, 29.31, 29.37, 29.56, 29.71, 31.64, 31.91, 31.94, 33.84, 65.54, 66.64, 66.94, 69.80, 69.85, 114.07, 115.93, 123.51, 124.06, 125.76, 125.93, 128.60, 131.66, 139.28 and 156.91. Anal. calcd for $C_{70}H_{72}Fe_2N_2O_4$: C, 75.27; H, 6.50; N, 2.51. Found: C, 75.33; H, 6.52; N, 2.52.

Synthesis of 2-((5-(2,5-bis-(n-decyl)-3,6-dioxo-4-(5-(ferrocenylethynyl)furan-2-yl)-2,3,5,6-tetrahydropyrrolo[3,4-c]pyrrol-1-yl)furan-2-yl)methylene)malononitrile ***9b*** *and (E)-2-(3-(2-(5-(2,5-bis-(n-decyl)-3,6-dioxo-4-(5-(ferrocenylethynyl)furan-2-yl)-2,3,5,6-tetrahydropyrrolo[3,4-c]pyrrol-1-yl)furan-2-yl)vinyl)-5,5-dimethylcyclohex-2-enylidene)malononitrile* ***9c***. A solution of **9a** (0.05 g, 0.06 mmol), piperidine (0.006 g, 0.07 mmol) anhydrous THF (10 ml) under inert atmosphere was cooled to 0 °C and a solution of malononitrile (0.008 g, 0.13 mmol) in anhydrous THF (1 ml) was added dropwise and the reaction stirred at 0 °C until completion (TLC). After extractive workup as described earlier, solvent was removed under reduced pressure to obtain crude **9b**, which was further purified by preparative TLC using 30 : 70 ($CHCl_3$/hexane) to isolate analytically pure bluish-green solid.

Similarly, using **9a** (0.06 g, 0.07 mmol), piperidine (0.008 g, 0.09 mmol) and 2-(3,5,5-trimethyl-2-cyclohexenylidene)malononitrile **10** (0.03 g, 0.15 mmol) and stirring the reaction at 40 °C for 24 h furnished **9c** as bluish green solid, after extractive work up of the reaction followed by purification as described above.

2-((5-(2,5-Bis-(n-decyl)-3,6-dioxo-4-(5-(ferrocenylethynyl)furan-2-yl)-2,3,5,6-tetrahydropyrrolo[3,4-c]pyrrol-1-yl)furan-2-yl)methylene)-malononitrile ***9b***. Yield: 65%. Mp 100–102 °C IR (KBr): ν_{max} 1099, 1398, 1531, 1600, 1660, 2198, 2228, 2854 and 2925 cm^{-1}. ^{1}H NMR (500 MHz, $CDCl_3$, 25 °C): δ (ppm) 0.85–0.88 (m, 6H, $-CH_3$), 1.23–1.29 (m, 28H, $-CH_2$), 1.74–1.77 (m, 4H, $-CH_2$), 4.16 (t, J = 7.5 Hz, 2H, $-CH_2$), 4.25–4.28 (br, 7H, Fc + 2 × CH_2), 4.36 (s, 2H, Fc), 4.57 (s, 2H, Fc), 6.72 (s, 1H, –CH =), 6.86 (d, J = 5 Hz, 1H, furanyl C4′–CH), 7.41 (d, J = 10 Hz, 1H, furanyl C3′–CH), 8.52 (d, J = 5 Hz, 1H, furanyl C4–CH) and 8.58 (d, J = 5 Hz, 1H, furanyl C3–CH). ^{13}C NMR (125 MHz, $CDCl_3$, 25 °C): δ (ppm) 14.11, 22.67, 26.62, 26.92, 29.29, 29.35, 29.46, 29.51, 29.55, 29.66, 29.70, 31.88, 42.22, 42.82, 62.47, 69.95, 70.33, 71.90, 98.76, 107.83, 118.09, 121.63, 124.80, 129.12, 135.27, 141.86, 143.51, 149.07, 150.18, 160.12 and 161.04. Anal. calcd for $C_{50}H_{56}FeN_4O_4$: C, 72.11; H, 6.78; N, 6.73. Found: C, 72.15; H, 6.73; N, 6.75.

(E)-2-(3-(2-(5-(2,5-Bis-(n-decyl)-3,6-dioxo-4-(5-(ferrocenylethynyl)-furan-2-yl)-2,3,5,6-tetrahydropyrrolo[3,4-c]pyrrol-1-yl)furan-2-yl)-vinyl)-5,5-dimethylcyclohex-2-enylidene)malononitrile ***9c***. Yield: 60%. Mp 88–90 °C IR (KBr): ν_{max} 1099, 1384, 1523, 1560, 1662, 2216, 2853 and 2924 cm^{-1}. ^{1}H (500 MHz, $CDCl_3$, 25 °C): δ (ppm) 0.85–0.88 (m, 6H, $-CH_2$), 1.09 (s, 6H, $-C(CH_3)_2$), 1.23–1.34 (m, 28H, $-CH_2$), 1.74–1.78 (m, 4H, $-CH_2$), 2.43 (s, 2H, $-CH_2$), 2.61 (s, 2H, $-CH_2$), 4.14–4.20 (m, 4H, $-CH_2$), 4.28 (s, 5H, Fc), 4.34 (s, 2H, Fc), 4.56 (s, 2H, Fc), 6.62 (d, J = 1.5 Hz, 2H, furanyl C4′–CH), 6.82–6.84 (m, 2H, –CH=CH–), 6.87 (s, 1H, furanyl C3′–CH), 8.37 (d, J = 5 Hz, 1H, furanyl C4–CH) and 8.41 (d, J = 5 Hz, 2H, furanyl C3–CH). ^{13}C NMR (125 MHz, $CDCl_3$, 25 °C): δ (ppm) 14.13, 22.69, 25.30, 26.96, 27.16, 27.82, 28.00, 29.37, 29.43, 29.52, 29.63, 29.68, 29.71, 30.26, 31.63, 31.93, 31.97, 32.37, 39.09, 42.64, 45.70, 62.88, 69.76, 70.28, 71.81, 78.29, 109.04, 112.39, 113.17, 117.83, 120.60, 122.32, 124.66, 129.58, 143.99, 145.97, 154.49, 159.70, 160.83 and 170.35. Anal. calcd for $C_{59}H_{68}FeN_4O_4$: C, 74.35; H, 7.19; N, 5.88. Found: C, 74.39; H, 7.22; N, 5.86.

Results and discussion

Synthesis and characterization

3,6-Di(furan-2-yl)-2,5-dihydropyrrolo[3,4-*c*]pyrrole-1,4-dione **1** (61%) was prepared from diisopropyl succinate and 2-furonitrile using a reported method.[50] Dialkylation of **1** was achieved by using *n*-decylbromide in anhydrous DMF at 120 °C (Scheme 1).[50] The resultant 2,5-bis-(*n*-decyl)-3,6-di(furan-2-yl)pyrrolo-[3,4-*c*]pyrrole-1,4(2*H*,5*H*)-dione **2** (48%) was then brominated (*vide experimental*) to obtain 3,6-bis-(5-bromofuran-2-yl)-2,5-bis-(*n*-decyl)-pyrrolo[3,4-*c*]pyrrole-1,4(2*H*,5*H*)dione **3** (58%) using bromine in chloroform. Intermediate **2** was then mono formylated using Vilsmeier–Haack reaction conditions to obtain 5-(2,5-bis-(*n*-decyl)-4-(furan-2-yl)-3,6-dioxo-2,3,5,6-tetrahydropyrrolo-[3,4-*c*]pyrrol-1-yl)furan-2-carbaldehyde **4** (50%) (Scheme 1).[66,67] Subsequent bromination of **4** using *N*-bromosuccinimide (NBS) in chloroform yielded 5-(4-(5-bromofuran-2-yl)-2,5-bis-(*n*-decyl)-3,6-dioxo-2,3,5,6-tetrahydropyrrolo[3,4-*c*]pyrrol-1-yl)furan-2-carbaldehyde **5** in good yield (71%) (Scheme 1).[68] Ethynylferrocene **8a**[69] (72%) and 4-(ethynylphenyl)ferrocene **8b**[70] (65%) were prepared (Scheme 2) using known methods.

Dyads of design A (Fig. 1) were easily prepared (Schemes 3–5) by Sonogashira coupling reaction[71,72] of 5-(4-(5-bromofuran-2-yl)-2,5-bis-(*n*-decyl-3,6-dioxo-2,3,5,6-tetrahydropyrrolo[3,4-*c*]-pyrrol-1-yl)furan-2-carbaldehyde **5** and ethynylferrocene **8a** using bis-triphenylphosphinedichloropalladium(II) and CuI as catalysts resulting in the formation of 5-(2,5-bis-(*n*-decyl)-3,6-dioxo-4-(5-(ferrocenylethynyl)furan-2-yl)-2,3,5,6-tetrahydropyrrolo-[3,4-*c*]pyrrol-1-yl)furan-2-carbaldehyde **9a** (45%) (Scheme 3). Dyad **9a** served as a common precursor for preparing the other two congeners of design A. Thus, Knoevenagal condensation reaction[23] of **9a** with malononitrile or 2-(3,5,5-trimethylcyclohex-2-enylidene)malononitrile **10** [57] in anhydrous THF (dried over benzophenoneketyl) and piperidine as base furnished 2-((5-(2,5-bis-(*n*-decyl)-3,6-dioxo-4-(5-(ferrocenylethynyl)furan-2-yl)-2,3,5,6-tetrahydropyrrolo[3,4-*c*]pyrrol-1-yl)furan-2-yl)methylene) malononitrile **9b** (65%) and (*E*)-2-(3-(2-(5-(2,5-bis-(*n*-decyl)-3,6-dioxo-4-(5-(ferrocenylethynyl)furan-2-yl)-2,3,5,6-tetrahydropyrrolo [3,4-*c*]pyrrol-1-yl)furan-2-yl)vinyl)-5,5-dimethylcyclohex-2-enylidene) malononitrile **9c** (60%) (Scheme 4), respectively. Similarly, Sonogashira coupling of **3** with **8a** led to the formation of 2,5-bis-(*n*-decyl)-3,6-bis-(5-(ferrocenylethynyl)furan-2-yl)pyrrolo[3,4-*c*]pyrrole-1,4(2*H*,5*H*)-dione **9e** (40%) (Scheme 5). Finally, Sonogashira coupling of **3** and **8b** furnished 3-(5-bromofuran-2-yl)-6-(5-((4-ferrocenylphenyl)ethynyl)furan-2-yl)-2,5-bis-(*n*-decyl)-2,5-dihydropyrrolo[3,4-*c*]pyrrole-1,4-dione **9d** (51%) (Scheme 5) in a synthetically useful manner. Dyad 3,6-bis-(5-((4-ferrocenyl) phenylethynyl)furan-2-yl)-2,5-bis-(*n*-decyl)-pyrrolo[3,4-*c*]pyrrole-1,4-(2*H*,5*H*)-dione **9f** (40%) was also isolated (Scheme 5) along with **9d**. All compounds were characterized using spectral techniques. The thermogravimetric analysis showed that **9a–9c** and **9e** are thermally stable up to 500 °C whereas, **9d** and **9f** show thermal stability up to 200 °C (see ESI Fig. S1†).

UV-visible absorption study

Chromophore **5** and dyads **9a–9f** show intense low energy (LE) charge transfer bands (MLCT or D–A) and weak intensity high

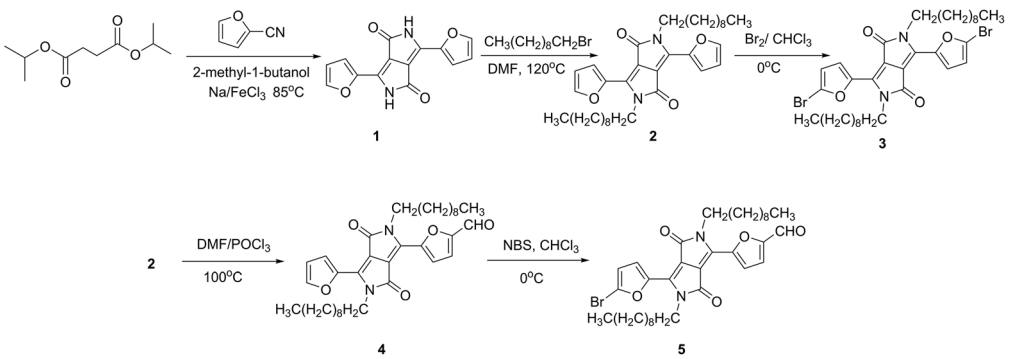

Scheme 1 Synthetic route to precursors **2**, **3** and **5**.

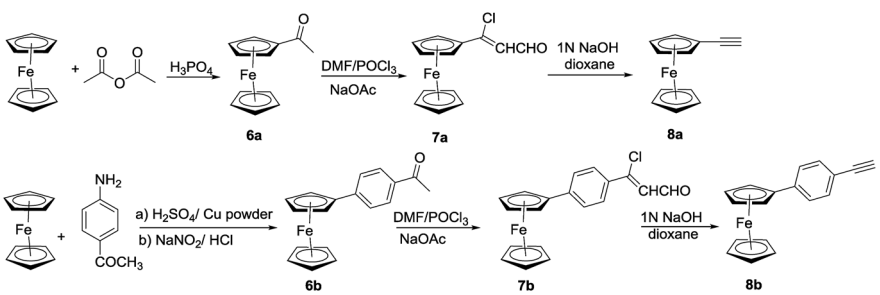

Scheme 2 Synthetic routes to precursors **8a**,**b**.

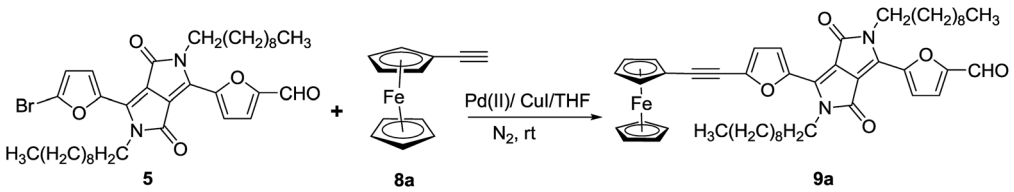

Scheme 3 Synthetic route to **9a**.

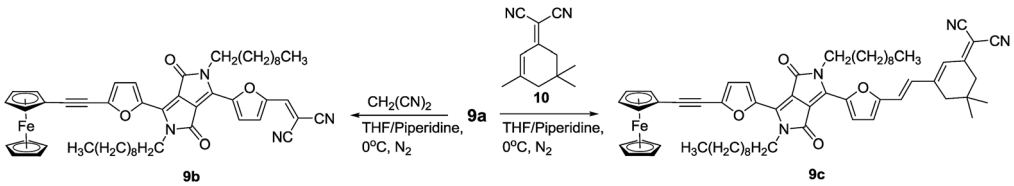

Scheme 4 Synthetic route to **9b** & **9c**.

energy (HE) bands (LMCT or π–π*) in the region of 500–700 nm and 300–450 nm, respectively, which are characteristic bands of DPP based chromophores.[55,73–79] Owing to extensive overlap, the absorption bands have been resolved using band fitting analysis (see ESI Fig. S2†), although typical LE (MLCT) and HE (ILCT) bands of the pristine Fc merged extensively with the HE and LE bands of the DPP core. However, on the basis of TD-DFT studies (carried using B3LYP/6-31G basis set and CPCM model using dichloromethane as solvent),[65] apparent contributions of the relevant transitions to the absorption bands have been assigned (see ESI Table S1†). The TD-DFT deduced FMOs of **5** & **9a–9f** and the associated energies are depicted in Fig. 2. The position of the LE CT bands of the dyads show a shift upon varying the strength of the acceptor as well as upon altering the length of the π-conjugation intervening D and A. Thus, the dipolar **9a–9c** show red shifted LE CT bands ($\Delta\lambda = 28$ nm, **5** → **9a**, $\Delta\lambda = 100$ nm, **5** → **9b**, $\Delta\lambda = 68$ nm, **5** → **9c**) w.r.t. the core **5** owing to the influence of the donor Fc and the acceptor moieties (Fig. 3). On increasing the acceptor strength from **9a** → **9c** → **9b**, a red shift is observed in the LE CT bands ($\Delta\lambda =$ 40 nm, **9a** → **9c**, $\Delta\lambda = 32$ nm, **9c** → **9b**). The red shift could be attributed to the stabilization of the LUMO energy as a consequence of increasing the acceptor strength from **9a** → **9c** → **9b**, whereas the energy of HOMO remains nearly the same (Table 1) in all these three dyads. The experimental linear optical data showed good correlation with the theoretical data. The latter also reveals that on increasing the strength of acceptor, the order of the stabilization of LUMO follows the same trend as obtained experimentally (Table 1). The LE CT band of **9d** and the disubstituted counterparts **9e** and **9f** displayed red shift ($\Delta\lambda = 28$ nm, **3** → **9d**, $\Delta\lambda = 52$ nm, **3** → **9e**, $\Delta\lambda$ $= 54$ nm, **3** → **9f**) w.r.t the position of the absorption band of the core **3**, which is attributable to the increase in the extent of π-conjugation. Both **9e** and **9f** have the same Fc donor, but the intervening π-conjugation is increased by the introduction of a phenyl ring (Fig. 4), which leads to a slight increase in energy of the HOMO in the latter, although optical band gap is nearly the same for both of these dyads (Table 1). As the extent of π-conjugation is increased from **9e** → **9f**, slight red shift is seen in the LE CT band ($\Delta\lambda = 2$ nm, **9e** → **9f**). Theoretical data also provides the evidence for this red shift as the calculated energy of HOMO is nearly the same for both **9e** and **9f** (Table 1), whereas LUMO of **9f** is more stabilized than that of **9e** leading to a decreased band gap of the former and the consequent red shift in the absorption band (Table 1). However, **9d** also shows a red shift as compared to **3** albeit of lower magnitude than observed in the pair of **9e** and **9f**. Evidently, the weak electron

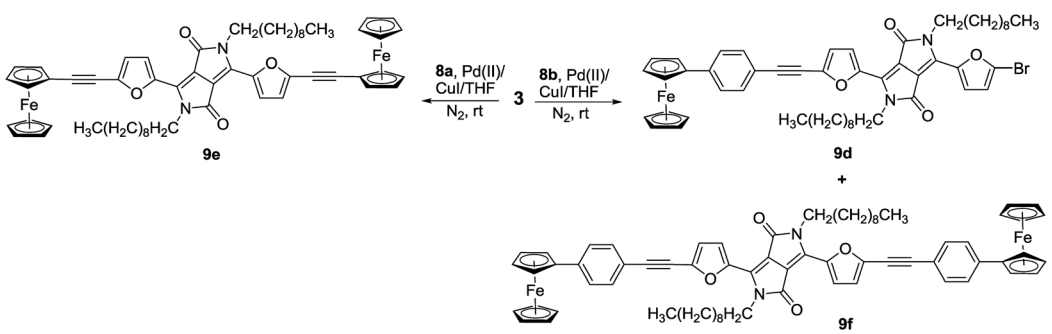

Scheme 5 Synthetic route to **9e**, **9d** & **9f**.

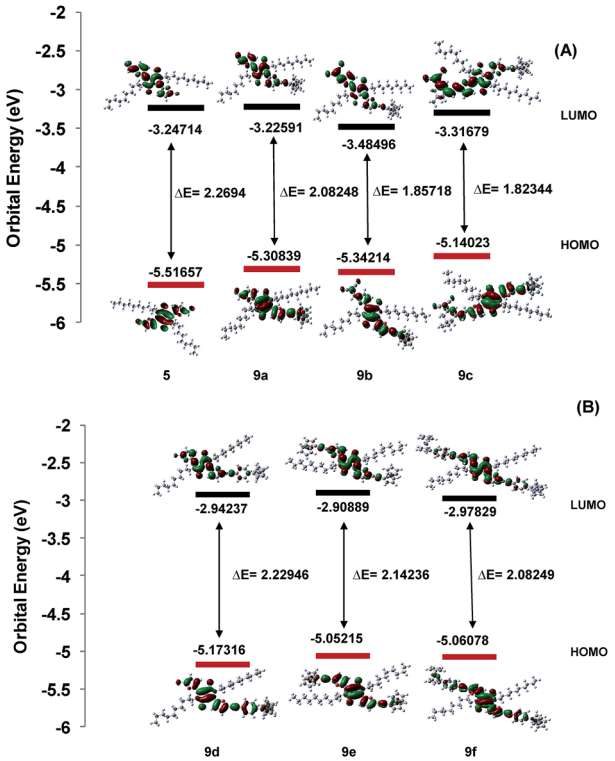

Fig. 2 Illustration of frontier molecular orbitals of **5**, **9a–9c** (A); **9d–9f** (B) at B3LYP/6-31G basis set.

donating nature of the Br group leads to an increased band gap as is also attested from the theoretical data (Table 1).

The dyads **9a–9f** show blue shift in LE CT band with the increase in the polarity of the solvent (see ESI Table S2†). The concentration dependence of the extinction coefficients was ruled out as no significant change in the relative intensity of the absorption bands was noticed when the absorption spectrum of the dipolar dyads **9b** and **9c** were recorded at five different concentrations ($1.2–6.0 \times 10^{-5}$ M (**9b**) and $0.9–4.7 \times 10^{-5}$ M (**9c**) in THF), which were also used in the HRS study (*vide infra*). Thus, the influence of aggregation in modulating the position of the absorption band and/or intensity has been ruled out. Hence, the observed shift in the absorption bands is attributed to solvatochromism. However, solvatochromism is only

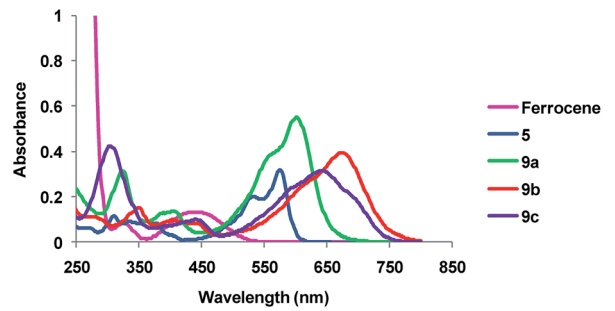

Fig. 3 Overlay of UV-visible spectra of **9a–9c** & **5** in dichloromethane at 1×10^{-5} M and Fc in dichloromethane at 1×10^{-3} M at 293 K.

significant in the dipolar dyads **9b** and **9c**, although it is negative, which suggests existence of a more polar ground state of these compounds compared to the corresponding excited states,[80–82] suggesting that the ground state is already a strong charge transfer state represented by the quinoidal forms (Fig. 5 and 6) as has indeed been described for similar dicyanovinyl chromophore.[83] The marginally higher bond length alternation (BLA)[83–85] of **9c** (Fig. 6) compared to shorter dyad **9b** suggests greater equalization of bond lengths in the latter, owing to the influence of the stronger dicyanovinyl acceptor. Thus, the dyads **9b** and **9c** were expected to show higher β-values in the present series of compounds. The observed more polar ground states of **9b** and **9c** also draw precedence from the literature, wherein the chromophores possessing MLCT ($d \rightarrow \pi^*$) and $n \rightarrow \pi^*$ transitions, depict an increase in the dipole moment of the ground state. This leads to hypsochromic shift of both the transitions on increasing the solvent polarity and has been ascribed to the electrostatic dipole–dipole interactions, which stabilize the ground state more than the excited state, resulting in a more dipolar ground state.[86] Also, polar protic solvents are capable of hydrogen bonding with the available lone pairs, hence stabilizing the ground state more than the excited state.[80]

Electrochemistry

Electrochemistry was performed in DCM (freshly distilled from CaH_2), with 2×10^{-2} M tetrabutyl ammonium hexafluorophosphate ($TBAPF_6$) as a supporting electrolyte (Aldrich, Electrochemical grade). A platinum electrode was used both as working as well as counter electrode and Ag/AgCl as reference electrode (CHI660D Electrochemical Workstation). All experiments were performed in N_2 purged solvent, and a N_2 gas blanket was maintained over the solution during the experiments. Fc was used as an internal reference. Voltammograms displayed in the paper were recorded with a scan rate of 100 mV s^{-1}. Variation in scan rates had minimal effect on peak potentials as well as in $E_{1/2}$ values. $E_{1/2}$ values are taken as the half-way point between the forward and reverse peak for each reversible redox process.

In analogy to the redox behaviour of Fc as well as the core **5**, dyads **9a–9f** show electrochemically reversible oxidation peaks (see ESI Fig. S10–S16†). Dyads **9a** and **9b** show nearly identical $E_{1/2}$ values with a negligible cathodic shift ($\Delta E_{1/2} = 0.002$ V, **9a** → **9b**), although the acceptor strength in the latter is large. This could be attributed to the slight difference in the energies of HOMO of both **9a** and **9b** (Table 1). However, **9c** shows a cathodic shift in the oxidation potential as compared to **9b** ($\Delta E_{1/2} = 0.018$ V, **9b** → **9c**) (Table 2) possibly due to decreased acceptor strength, increased intervening π-conjugation in the former and the marginally higher energy of the HOMOs (Table 1). Similarly, the disubstituted chromophores also show cathodic shift in $E_{1/2}$ on increasing π-conjugation from **9e** → **9f** ($\Delta E^{I}_{1/2} = 0.136$ V, $\Delta E^{II}_{1/2} = 0.099$ V) (Table 2) due to rise in energy of HOMO of **9f**. However, **9d** shows anodic shift in $E_{1/2}$ w.r.t. **9f** ($\Delta E^{I}_{1/2} = 0.023$ V, $\Delta E^{II}_{1/2} = 0.034$ V **9d** → **9f**) (Table 2), which could be attributed to the stabilization of HOMO of **9d** due to the decreased π-conjugation

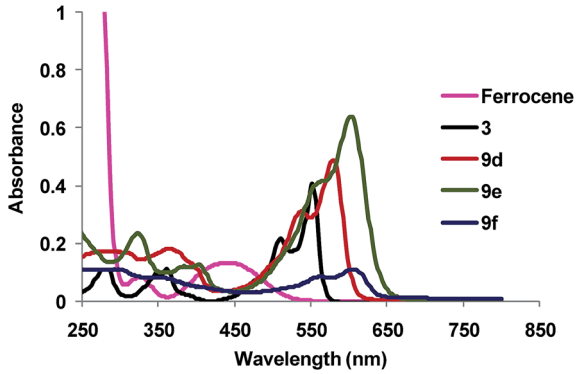

Fig. 4 Overlay of UV-visible spectra of **9d–9f** & **3** in dichloromethane at 1×10^{-5} M and Fc in dichloromethane at 1×10^{-3} M at 293 K.

in **9d**, indicative of an increased electronic communication between donor and acceptor. Theoretical data also correlates well with the experimental observation. Further, whereas in **9a**, an additional reversible oxidation wave corresponding to the core **5** was observed at $E_{1/2}$ 1.148 V, the same was not observed in both **9b** and **9c**, which also suggests these dyads to be efficient D–A systems owing to the increased strength of the acceptors. Similarly, **9e** and **9f** represent disubstituted analogues with D–A–D type constitution and consequently show an additional reversible oxidation peak at $E_{1/2}$ 1.056 V and 0.957 V (Table 2), respectively, attributable to the DPP unit. Dyad **9d** however, shows two reversible oxidation peaks at $E_{1/2}$ 0.992 V and 1.343 V, respectively, in a manner similar to **5**, in addition to the redox wave of Fc donor. Further, the amplitude of the cathodic peak of the one Fc unit containing **9a**, that correspond to a single electron redox process was roughly doubled (Table 2) in case of **9e** and **9f** that contain two Fc units.

Computational studies

The molecular geometries of the dyads were optimized on B3LYP/6-31G level along with the TD-DFT calculations using same basis set in gas phase as well as in solvent medium using CPCM model to get a deeper insight into the effect of varying donor, acceptor and the extent of π-conjugation on the dipole moment, second-order nonlinear polarizability (β) and other related properties.[65] The calculated HOMO–LUMO band gaps show a good correlation with the optical band gaps obtained from CV and UV-visible absorption data (Table 1 & see ESI Fig. S17†). The calculated energies of the sets of HOMO and LUMO (see ESI Tables S3 & S4†) of the dyads show good correlation with experimental data as discussed in the above sections. The plots of FMOs (see ESI Fig. S18†) reveal that HOMO–LUMO band gap is modulated possibly by both the strength of the acceptors as well as the length of the π-conjugation. Thus, **9b** appended with a stronger dicyanovinyl acceptor shows HOMO–LUMO band gap (ΔE = 1.85718 eV) comparable to **9c** (ΔE = 1.82344 eV), appended with a relatively weaker acceptor through a longer π-conjugation bridge even as a minor stabilization of LUMOs of **9f** (E_L = −2.97829 eV) bearing a longer π-conjugation was observed compared to **9e** (E_L = −2.90889 eV) (Table 1 and Fig. 2). The contour plots of the orbitals involved in the transitions are shown in Fig. S19 and S20 (see ESI†) and tentative assignment to the electronic transitions is made (see ESI Table S1†). In the dipolar dyads **9a–9c**, LE transition is assigned as D → A CT transition in which HOMO is mainly localised on Fc unit along with small contributions from the π-bridge and DPP unit, whereas the electron density is shifted towards the acceptor showing the LUMO mainly located on the acceptor along with some contributions from the π-bridge and DPP unit. However, H-2 → LUMO also shows contribution to LE D → A CT transition in **9a**. Similarly,

Table 1 Comparison of experimental (CV/UV-visible) and the calculated (TD-DFT) HOMO–LUMO energy data and dipole moments of **5** & **9a–9f**

	Experimental data			TD-DFT calculations[a]			
Compound	E_{HOMO}[b] (eV)	$E_g^{opticalc}$ (eV)	E_{LUMO}[d] (eV)	E_{HOMO} (eV) TD-DFT gas phase/ solvent phase	E_{LUMO} (eV) TD-DFT gas phase/ solvent phase	ΔE (eV) TD-DFT gas phase/ solvent phase	μ TD-DFT gas phase/solvent phase
5	−5.464	2.066	−3.398	−5.48718/ −5.51657	−3.22808/ −3.24714	2.2591/ 2.2694	4.9102/ 6.1060
9a	−5.012	1.913	−3.099	−5.20853/ −5.30839	−3.10427/ −3.22591	2.104026/ 2.08248	8.6296/ 10.5140
9b	−5.03	1.657	−3.373	−5.34948/ −5.34214	−3.47543/ −3.48496	1.87405/ 1.85718	13.2713/ 15.7635
9c	−5.00	1.675	−3.325	−5.07601/ −5.14023	−3.31788/ −3.31679	1.75813/ 1.82344	11.5754/ 13.7962
9d	−4.925	2.066	−2.859	−4.99301/ −5.17316	−2.75705/ −2.94237	2.23596/ 2.22946	3.7068/ 4.3492
9e	−5.012	1.937	−3.075	−4.79628/ −5.0515	−2.64494/ −2.90889	2.15134/ 2.14236	0.2513/ 0.2931
9f	−4.85	1.943	−2.907	−4.82267/ −5.06078	−2.73256/ −2.97829	2.09011/ 2.08249	0.2685/ 0.3874

[a] B3LYP/6-31G level. [b] Calculated as $E_{HOMO} = -e[E_{ox}^{onset} + 4.4]$. [c] Calculated as $E_g^{optical} = 1239.84187/\lambda_{onset}$. [d] Calculated as $E_{LUMO} = E_g^{optical} + E_{HOMO}$.

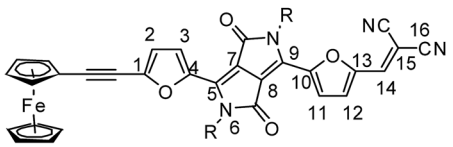

9b

(where bond lengths (Å): 1→2 = 1.3880; 2→3 = 1.4145; 3→4 = 1.3896; 4→5 = 1.4917; 5→6 = 1.3988; 5→7 = 1.4021; 7→8 = 1.4166; 8→9 = 1.3966; 9→10 = 1.4230; 10→11 = 1.3944; 11→12 = 1.4104; 12→13 = 1.3936; 13→14= 1.4158; 14→15 = 1.3786; 15→16 = 1.4273).

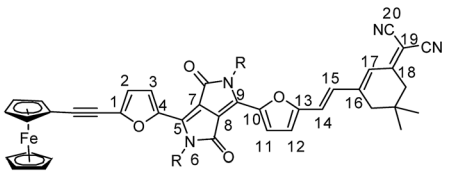

9c

(where bond lengths (Å): 1→2 = 1.3970; 2→3 = 1.4157; 3→4 = 1.3887; 4→5 = 1.4210; 5→6 = 1.4004; 5→7 = 1.3997; 7→8 = 1.418; 8→9 = 1.3971; 9→10 = 1.4217; 10→11 = 1.3931; 11→12 = 1.4132; 12→13 = 1.3913; 13→14 = 1.4222; 14→15 = 1.3665; 15→16 = 1.4481; 16→17 = 1.3760; 17→18 = 1.4317; 18→19 = 1.3908; 19→20 = 1.4274).

Fig. 5 DFT/B3LYP/6-31G optimized bond lengths (in Å) of **9b** and **9c**.

in the disubstituted chromophores **9e** and **9f,** the LE transitions are assigned as HOMO → LUMO (MLCT) transitions since the HOMO is mainly located on Fc unit with small contribution from π-bridge and DPP unit, whereas the LUMO is mainly located on DPP unit with small contribution from π-bridge (the contour plots show increased electron density on the DPP unit). On the similar basis, LE transition in **9d** is assigned as HOMO → LUMO CT (MLCT) transition. These LE CT transitions show higher oscillator strength (*f*) (see ESI Table S1†) than that of HE transitions. The HE transitions are expected to have contributions from multiple transitions *i.e.* LMCT, π–π*, A → D or intraligand CT transitions (see ESI Table S1†). Thus, HOMO → LUMO transitions correspond to LE CT absorption bands in all the chromophores except in **9a** in which H-2 → LUMO also contributes to LE CT absorption band. Further, it has been observed that HE transitions in **9c** with relatively large *f*-values also correspond to D → A CT transition as visualized from the contour plots of the orbitals (see ESI Fig. S19†). Thus, the charge transfer is expected to increase due to the contributions from both HE (H-3 → LUMO & H-4 → LUMO) and LE (HOMO → LUMO) CT transitions, thus β is expected to be largest for **9c**.

The calculated values of dipole moments (μ) in gas phase as well as in solvent phase correlate well with the structures of the dyads (Table 1). The central core **5**, being a strong acceptor shows a large dipole moment. On increasing the acceptor strength from **9a** → **9c** → **9b**, the dipole moment shows the same trend. Similarly, dipolar analogue **9d** also shows dipole moment greater than that of **9e** and **9f** (Table 1). However, the symmetrically substituted **9e** and **9f** have non-zero dipole moment (Table 1), indicating their non-centrosymmetric

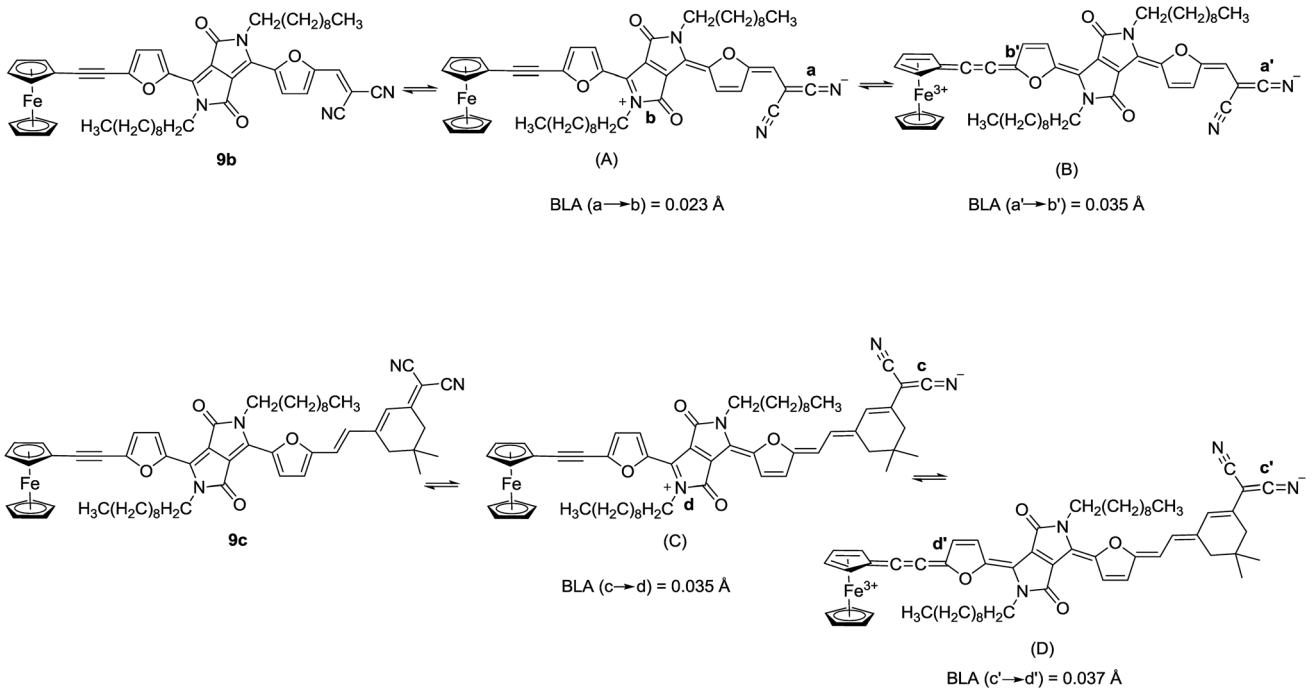

Fig. 6 Depiction of possible quinoid like structures (A–D) of **9b** and **9c**.

Table 2 Electrochemical data for Fc, 5 & 9a–9f in CH_2Cl_2[a]

Compound	E_{pa} (V)	E_{pc} (V)	$E_{1/2}$ (V)	i_{pa}[b] $\times 10^{-6}$ (A)	i_{pc}[b] $\times 10^{-6}$ (A)
Fc	0.572	0.472	0.522	−2.116	−2.180
5	1.176	1.070	1.123	−0.902	0.379
	1.496	1.406	1.451	−1.897	−0.279
9a	0.760	0.640	0.700	−0.788	0.868
	1.208	1.089	1.148	−0.813	−0.295
9b	0.748	0.648	0.698	−0.074	0.085
9c	0.725	0.635	0.680	−0.107	0.089
9d	0.637	0.526	0.581	−2.188	2.091
	1.043	0.941	0.992	−1.596	1.291
	1.394	1.293	1.343	−2.063	−0.938
9e	0.751	0.638	0.694	−1.700	1.749
	1.106	1.006	1.056	−0.759	0.432
9f	0.601	0.516	0.558	−0.979	1.892
	1.004	0.910	0.957	−0.510	0.229

[a] Half-wave potential, $E_{1/2} = (E_{pc} + E_{pa})/2$, where E_{pc} and E_{pa} correspond to the cathodic and anodic peak potentials, respectively; ΔE_p = 80–120 mV; and a scan rate of 100 mV s^{-1}. [b] Amplitudes of the anodic and cathodic peaks.

nature. The optimised geometries of **9e** and **9f** (Fig. S21†) show slight distortion from the planarity leading to non-zero dipole moments. As **9f** is slightly more distorted than **9e**, **9f** has slightly larger dipole moment (Table 1). Hence, non-zero second-order nonlinear polarizability values are expected for both disubstituted dyads **9e** and **9f**. On the basis of calculated dipole moments, notations are assigned to these dyads: d–A–a (**5**); D–s–A–a (**9a**); D–s–A–A′ (**9b**); D–s–A–A″ (**9c**); D–l–A–d (**9d**); D–s–A–s–D (**9e**) and D–l–A–l–D (**9f**), where d-weak donor (Br); a-weak acceptor (CHO); D-strong donor (Fc); A-strong acceptor (central unit); s-short conjugated bridge; l-long conjugated bridge and A′ or A″-dicyanovinyl acceptors. β values are in agreement with the dipole moments except **9b** and **9c**.

Quadratic hyperpolarizability

The second-order nonlinear polarizabilities, β, of **9a–9f** were measured for dilution series (10^{-5} to 10^{-4} M) in THF at 840 nm using HRS method[59–64] under ambient conditions. The octopolar symmetry[27,28,87] of the reference crystal violet was appropriately taken care of and the difference in solvent was corrected for by the optical local field correction factors. A multiphoton fluorescence discrimination technique in the frequency domain has been applied. Only for the DPP core **5**, multiphoton fluorescence at 420 nm was contributing to the scattering signal. With the high frequency demodulation technique, it was possible to obtain an accurate fluorescence-free second-order nonlinear polarizability value. The concentration range used for the nonlinear experiments was small enough to preclude any aggregation effects. The photostability (under femtosecond pulsed 840 nm laser light) was checked by comparing absorbance before and after the nonlinear experiment and no differences were observed.

The principle factors, which determine the degree of polarization are strength of donor and acceptor as well as the intervening π-conjugation bridge.[2,12,27,88–94] According to the two-level model (eqn (1)):[95,96]

$$\beta \propto \Delta\mu_{ge} r_{ge}^2/(E_{ge})^2 \quad (1)$$

where, β = second-order nonlinear polarizability. $\Delta\mu_{ge}$ = difference in excited state and ground state dipole moments. r_{ge} = transition dipole moment, which can be directly correlated to oscillator strength (f) or molar extinction coefficient (ϵ). E_{ge} = LE CT transition band gap.

Dyad **9c** shows a greater β value as compared to **9a** and **9b** compared to the central DPP core **5**. The order of the β values for the dyads is: **9c** > **9b** > **9a** (Table 3), although, **9b** is appended with a stronger dicyanovinyl electron acceptor compared to **9c** as inferred from the trend (**9b** > **9c** > **9a**, Table 1) of the calculated (TD-DFT: B3LYP/6-31G) dipole moments in DCM medium. As the acceptor strength increases from **9a** → **9b**, whereas, the calculated band gap decreases (Table 1), the oscillator strength (f) of CT band shows an increasing trend (see ESI Table S1†), which could account for the observed trend (**9b** > **9a**) of the β values (Table 3). However, **9c** shows exceptionally high β (Table 3) as compared to **9b**, although the former has a weaker acceptor as well as smaller dipole moment (Table 1). This could be attributed to the high oscillator strength of charge transfer LE absorption band (see ESI Table S1†) in **9c**, as well as there is marginal increase in energy of the HOMOs in **9c** owing to longer conjugation. Further, in addition to the LE CT absorption band in **9c**, HE band at 306 nm also corresponds to D → A CT transition as depicted from the FMO diagram (see ESI Fig. S19†). Thus, both HE and LE absorption bands are expected to contribute to the charge transfer and the associated larger β. Similarly, in disubstituted analogues **9e** and **9f**, the observed trend in the β values: **9f** > **9e** (Table 3) is attributable to the increase in the π-conjugation bridge. Further, **9e** and **9f** were expected to have zero dipole moments but the optimized geometries (Fig. S21†) revealed slight distortion of the molecular planarity, leading to non-zero dipole moments and hence non-zero β. Also, **9f** has higher oscillator strength (f) of CT band as well as lower band gap as compared to **9e**, which may also be an additional contributory factor in the higher β value in the former. However, **9d** shows higher β than both **9e** and **9f** (Table 3), irrespective of its higher band gap (Table 1) and lower

Table 3 Quadratic nonlinear optical parameters of 5 & 9a–9f

Compound	β_{HRS}[a] (10^{-30} esu)	$\beta_{HRS,0}$[b] (10^{-30} esu)
5	68 ± 4	31 ± 2
9a	207 ± 8	104 ± 4
9b	303 ± 13	170 ± 7
9c	913 ± 30	502 ± 6
9d	173 ± 8	81 ± 4
9e	152 ± 9	77 ± 5
9f	160 ± 8	82 ± 4

[a] Second-order nonlinear polarizability, β_{HRS} recorded at 840 nm in THF. [b] Second-order nonlinear polarizability corrected for resonance enhancement, $\beta_{HRS,0}$.

oscillator strength (f) of CT band (see ESI Table S1†). It could be explained on the basis of increased dipole moment (Table 1) in this dipolar congener, leading to increase in charge transfer and hence higher β.

Conclusions

Synthesis of new ferrocene-DPP dyads has been described. Femtosecond HRS measurements were performed at 840 nm using a commercial Ti : sapphire laser at ambient temperature and revealed structure dependent high quadratic hyperpolarizabilities. As deduced from the UV-visible absorption, electrochemical, theoretical calculations, the second-order nonlinear polarizability, β, increased on increasing both, the strength of acceptor as well as the length of the intervening π-conjugated linker, although the effect of former was more pronounced. This is in contrast to our earlier[23] finding, wherein the β-values of ferrocene dyads were significantly modulated upon increasing the length of the π-conjugated chain connecting the ferrocene donor with an acceptor. Also, the LE CT bands of the dipolar (D–A) dyads D–s–A–a (**9a**); D–s–A–A′ (**9b**); D–s–A–A″ (**9c**), where a-weak acceptor (CHO); D-strong donor (Fc); A-strong acceptor (central unit); s-short conjugated bridge; l-long conjugated bridge and A′ or A″-dicyaovinyl acceptors, appeared at lower energy as well as showed smaller HOMO–LUMO band gaps as compared to the disubstituted dyads, D–s–A–s–D (**9e**) and D–l–A–l–D (**9f**). Further, these dyads showed negative solvatochromism. Further, the cyclic voltammograms of the dipolar dyads **9b** and **9c** showed only one reversible oxidation peak corresponding to the one-electron oxidation of the Fc unit. However, the oxidation peaks of the disubstituted dyads **9e** and **9f** observed a cathodic shift as well as possessed roughly doubled amplitude due to two Fc units, compared to that of the dipolar dyad **9a**. Additionally, the disubstituted dyads showed non-zero dipole moments, indicating their non-centrosymmetric nature and hence non-zero quadratic hyperpolarizabilities. A good correlation of the structural changes of the dyads as well as effect of substituents with the experimental β-values was established. From the point of view of the development of electrooptic devices and applications, these new, thermally stable DPP based dyads represent a good strategy for further exploration.

Acknowledgements

We are thankful to SERB-DST, New Delhi for the project SB/S1/OC-45/2013 as well as CSIR, New Delhi for research fellowships to SK and SD.

Notes and references

1 N. J. Long, *Angew. Chem., Int. Ed. Engl.*, 1995, **34**, 21–38.
2 D. R. Kanis, M. A. Ratner and T. J. Marks, *Chem. Rev.*, 1994, **94**, 195–242.
3 S. R. Marder, B. Kippelen, A. K.-Y. Jen and N. Peyghambarian, *Nature*, 1997, **388**, 845–851.
4 I. R. Whittall, A. M. McDonagh, M. G. Humphrey and M. Samoc, *Adv. Organomet. Chem.*, 1998, **42**, 291–362.
5 K. A. Green, M. P. Cifuentes, M. Samoc and M. G. Humphrey, *Coord. Chem. Rev.*, 2011, **255**, 2025–2038.
6 P. N. Prasad and D. J. Williams, *Nonlinear Optical Effects in Molecules and Polymers*, Wiley, New York, 1991.
7 P. N. Prasad, *Nonlinear Optical Properties of Organic Materials*, Plenum, New York, 1991.
8 P. N. Prasad, *Nanophotonics*, Wiley, New York, 2004.
9 R. W. Boyd, *Nonlinear Optics*, Academic Press, New York, 1992.
10 Y. Shirota, *J. Mater. Chem.*, 2000, **10**, 1–25.
11 K. Clays, *Chem. Mater.*, 2003, **15**, 642–648.
12 M. G. Kuzyk, *J. Mater. Chem.*, 2009, **19**, 7444–7465.
13 S. R. Marder, D. N. Beratan and L.-T. Cheng, *Science*, 1991, **252**, 103–106.
14 M. Lamrani, R. Hamasaki, M. Mitsuishi, T. Miyashitab and Y. Yamamoto, *Chem. Commun.*, 2000, 1595–1596.
15 C. E. Powell and M. G. Humphrey, *Coord. Chem. Rev.*, 2004, **248**, 725–756.
16 S. Barlow and S. R. Marder, *Chem. Commun.*, 2001, 1555–1562.
17 P. Debroy and S. Roy, *Coord. Chem. Rev.*, 2007, **251**, 203–221.
18 R. Horikoshi and T. Mochida, *Eur. J. Inorg. Chem.*, 2010, 5355–5371.
19 T. Weyland, I. Ledoux, S. Brasselet, J. Zyss and C. Lapinte, *Organometallics*, 2000, **19**, 5235–5237.
20 C. Sporer, I. Ratera, D. Ruiz-Molina, Y. Zhao, J. Vidal-Gancedo, K. Wurst, P. Jaitner, K. Clays, A. Persoons, C. Rovira and J. Veciana, *Angew. Chem., Int. Ed.*, 2004, **43**, 5266–5268.
21 M. Samoc, N. Gauthier, M. P. Cifuentes, F. Paul, C. Lapinte and M. G. Humphrey, *Angew. Chem., Int. Ed.*, 2006, **45**, 7376–7379.
22 B. J. Coe, *Acc. Chem. Res.*, 2006, **39**, 383–393.
23 P. Kaur, M. Kaur, G. Depotter, S. van Cleuvenbergen, I. Asselberghs, K. Clays and K. Singh, *J. Mater. Chem.*, 2012, **22**, 10597–10608.
24 W.-Y. Wang, N.-N. Ma, S.-L. Sun and Y.-Q. Qiu, *Phys. Chem. Chem. Phys.*, 2014, **16**, 4900–4910.
25 M. D. Ward, *Chem. Soc. Rev.*, 1995, **24**, 121–134.
26 T. Kuwana, D. E. Bublitz and G. L. K. Hoh, *J. Am. Chem. Soc.*, 1960, **82**, 5811–5817.
27 T. Verbiest, S. Houbrechts, M. Kauranen, K. Clays and A. Persoons, *J. Mater. Chem.*, 1997, **7**, 2175–2189.
28 S. D. Bella, *Chem. Soc. Rev.*, 2001, **30**, 355–366.
29 Y. Liao, S. Bhattacharjee, K. A. Firestone, B. E. Eichinger, R. Paranji, C. A. Anderson, B. H. Robinson, P. J. Reid and L. R. Dalton, *J. Am. Chem. Soc.*, 2006, **128**, 6847–6853.
30 N. Tsuboya, M. Lamrani, R. Hamasaki, M. Ito, M. Mitsuishi, T. Miyashita and Y. Yamamoto, *J. Mater. Chem.*, 2002, **12**, 2701–2705.
31 N. Tsuboya, R. Hamasaki, M. Ito, M. Mitsuishi, T. Miyashitab and Y. Yamamoto, *J. Mater. Chem.*, 2003, **13**, 511–513.
32 Y. Lin, P. Cheng, Y. Liu, Q. Shi, W. Hu, Y. Li and X. Zhan, *Org. Electron.*, 2012, **13**, 673–680.

33 D. Deng, Y. Yang, J. Zhang, C. He, M. Zhang, Z.-G. Zhang, Z. Zhang and Y. Li, *Org. Electron.*, 2011, **12**, 614–622.
34 S. Qu and H. Tian, *Chem. Commun.*, 2012, **48**, 3039–3051.
35 B. Walker, J. Liu, C. Kim, G. C. Welch, J. K. Park, J. Lin, P. Zalar, C. M. Proctor, J. H. Seo, G. C. Bazan and T.-Q. Nguyen, *Energy Environ. Sci.*, 2013, **6**, 952–962.
36 M. J. Robb, S.-Y. Ku, F. G. Brunetti and C. J. Hawker, *J. Polym. Sci., Part A: Polym. Chem.*, 2013, **51**, 1263–1271.
37 S.-Y. Liu, W.-Q. Liu, J.-Q. Xu, C.-C. Fan, W.-F. Fu, J. Ling, J.-Y. Wu, M.-M. Shi, A. K.-Y. Jen and H.-Z. Chen, *ACS Appl. Mater. Interfaces*, 2014, **6**, 6765–6775.
38 Y.-W. Su, S.-C. Lan and K.-H. Wei, *Mater. Today*, 2012, **15**, 554–562.
39 T. Beyerlein, B. Tieke, S. F. Lenger and W. Brutting, *Synth. Met.*, 2002, **130**, 115–119.
40 D. Cao, Q. Liu, W. Zeng, S. Han, J. Peng and S. Liu, *Macromolecules*, 2006, **39**, 8347–8355.
41 A. C. Grimsdale, K. L. Chan, R. E. Martin, P. G. Jokisz and A. B. Holmes, *Chem. Rev.*, 2009, **109**, 897–1091.
42 S.-L. Suraru, U. Zschieschang, H. Klauk and F. Wurthner, *Chem. Commun.*, 2011, **47**, 1767–1769.
43 Y. Qiao, Y. Guo, C. Yu, F. Zhang, W. Xu, Y. Liu and D. Zhu, *J. Am. Chem. Soc.*, 2012, **134**, 4084–4087.
44 A. K. Palai, J. Lee, S. Das, J. Lee, H. Cho, S.-U. Park and S. Pyo, *Org. Electron.*, 2012, **13**, 2553–2560.
45 T. L. Chen, Y. Zhang, P. Smith, A. Tamayo, Y. Liu and B. Ma, *ACS Appl. Mater. Interfaces*, 2011, **3**, 2275–2280.
46 Y. Lin, L. Ma, Y. Li, Y. Liu, D. Zhu and X. Zhan, *Adv. Energy Mater.*, 2013, **3**, 1166–1170.
47 Y. Lin, Y. Li and X. Zhan, *Adv. Energy Mater.*, 2013, **3**, 724–728.
48 S. Qu, W. Wu, J. Hua, C. Kong, Y. Long and H. Tian, *J. Phys. Chem. C*, 2010, **114**, 1343–1349.
49 S. Qu, C. Qin, A. Islam, Y. Wu, W. Zhu, J. Hua, H. Tian and L. Han, *Chem. Commun.*, 2012, **48**, 6972–6974.
50 Y. Li, P. Sonar, S. P. Singh, W. Zeng and M. S. Soh, *J. Mater. Chem.*, 2011, **21**, 10829–10835.
51 S.-S. Li, K.-J. Jiang, F. Zhang, J.-H. Huang, S.-G. Li, M.-G. Chen, L.-M. Yang and Y.-L. Song, *Org. Electron.*, 2014, **15**, 1579–1585.
52 M. Shahid, T. McC-Ward, J. Labram, S. Rossbauer, E. B. Domingo, S. E. Watkins, N. Stingelin, T. D. Anthopoulosb and M. Heeney, *Chem. Sci.*, 2012, **3**, 181–185.
53 W. Li, W. S. C. Roelofs, M. M. Wienk and R. A. J. Janssen, *J. Am. Chem. Soc.*, 2012, **134**, 13787–13795.
54 A. N. Krol, M. Grzybowski, J. Romiszewski, M. Drobizhev, G. Wicks, M. Chotkowski, A. Rebane, E. Gorecka and D. T. Gryko, *Chem. Commun.*, 2013, **49**, 8368–8370.
55 A. D. Hendsbee, J.-P. Sun, L. R. Rutledge, I. G. Hillb and G. C. Welch, *J. Mater. Chem. A*, 2014, **2**, 4198–4207.
56 M. M. Hale, Creative Commons Attribution License (CC-BY 2.0).
57 H. Chun, I. K. Moon, D.-H. Shin and N. Kim, *Chem. Mater.*, 2001, **13**, 2813–2817.
58 A. M. McDonagh, N. T. Lucas, M. P. Cifuentes, M. G. Humphrey, S. Houbrechts and A. Persoons, *J. Organomet. Chem.*, 2000, **605**, 184–192.
59 K. Clays and A. Persoons, *Phys. Rev. Lett.*, 1991, **66**, 2980–2983.
60 K. Clays and A. Persoons, *Rev. Sci. Instrum.*, 1992, **63**, 3285–3289.
61 K. Clays, A. Persoons and L. de Maeyer, *Adv. Chem. Phys.*, 1994, **85**, 455–498.
62 K. Clays and A. Persoons, *Rev. Sci. Instrum.*, 1994, **65**, 2190–2194.
63 G. Olbrechts, R. Strobbe, K. Clays and A. Persoons, *Rev. Sci. Instrum.*, 1998, **69**, 2233–2241.
64 G. Olbrechts, K. Wostyn, K. Clays and A. Persoons, *Opt. Lett.*, 1999, **24**, 403–405.
65 M. J. Frisch, *et al.*, *Gaussian 09, Revision B.01*, Gaussian, Inc., Wallingford, CT, 2010 (for complete reference see ESI)†
66 I. M. Downie, M. J. Earle, H. Heaney and K. F. Shuhaibar, *Tetrahedron*, 1993, **49**, 4015–4034.
67 V. Nair, S. Thomas, S. C. Mathew, N. Vidya and N. P. Rath, *Tetrahedron*, 2005, **61**, 9533–9540.
68 J. C. Bijleveld, B. P. Karsten, S. G. J. Mathijssen, M. M. Wienk, D. M. de Leeuw and R. A. J. Janssen, *J. Mater. Chem.*, 2011, **21**, 1600–1606.
69 J. Polin and H. Schottenberger, *Org. Synth.*, 1998, **9**, 411.
70 B. J. Coe, C. J. Jones and J. A. McCleverty, *J. Organomet. Chem.*, 1994, **464**, 225–232.
71 R. Chinchill and C. Najera, *Chem. Rev.*, 2007, **107**, 874–922.
72 R. Chinchilla and C. Najera, *Chem. Soc. Rev.*, 2011, **40**, 5084–5121.
73 J. B. Lee, K. H. Kim, C. S. Hong and D. H. Choi, *J. Polym. Sci., Part A: Polym. Chem.*, 2012, **50**, 2809–2818.
74 S.-S. Li, K.-J. Jiang, F. Zhang, J.-H. Huang, S.-G. Li, M.-G. Chen, L.-M. Yang and Y.-L. Song, *Org. Electron.*, 2014, **15**, 1579–1585.
75 C.-Y. Ji, L. Yin, L. Wang, T. Jia, S. Meng, Y. Sun and Y. Li, *J. Mater. Chem. C*, 2014, **2**, 4019–4026.
76 Y. Kim, C.-E. Song, A. Cho, J. Kim, Y. Eom, J. Ahn, S.-J. Moon and E. Lim, *Mater. Chem. Phys.*, 2014, **143**, 825–829.
77 J. Dhar, N. Venkatramaiah, A. Anitha and S. Patil, *J. Mater. Chem. C*, 2014, **2**, 3457–3466.
78 Y. S. Park, T. S. Kale, C.-Y. Nam, D. Choi and R. B. Grubbs, *Chem. Commun.*, 2014, **50**, 7964–7967.
79 Z. Deng, L. Chen, F. Wu and Y. Chen, *J. Phys. Chem. C*, 2014, **118**, 6038–6045.
80 S.-H. Choi, O.-T. Kwon, N.-R. Kim, C. Yoon, J.-P. Kim and J.-H. Choi, *Bull. Korean Chem. Soc.*, 2010, **31**, 1073–1076.
81 S. Lunak Jr, M. Vala, J. Vynuchal, I. Ouzzane, P. Horakova, P. Moziskova, Z. Elias and M. Weiter, *Dyes Pigm.*, 2011, **91**, 269–278.
82 R. S. Szabadai, J. R. Barton, K. P. Ghiggino, J. M. White and D. J. D. Wilson, *Aust. J. Chem.*, 2014, **67**, 1330–1337.
83 M. C. R. Delgado, V. Hernandez, J. Casado, J. T. L. Navarrete, J. M. Raimundo, P. Blanchard and J. Roncali, *Chem.–Eur. J.*, 2003, **9**, 3670–3682.
84 R. Andreu, M. J. Blesa, L. Carrasquer, J. Garin, J. Orduna, B. Villacampa, R. Alcala, J. Casado, M. C. R. Delgado,

J. T. L. Navarrete and M. Allain, *J. Am. Chem. Soc.*, 2005, **127**, 8835–8845.
85 G. Y. Wang, Y. H. Kan, Y. Geng, Y. A. Duan, L. Wang, H. Q. Wu, X. X. Dong and Z. M. Su, *Theor. Chem. Acc.*, 2014, **133**, 1453.
86 C. Reichardt, *Solvents and Solvent Effects in Organic Chemistry*, Wiley-VCH, edn 3rd, 2003.
87 H. M. Kim and B. R. Cho, *J. Mater. Chem.*, 2009, **19**, 7402–7409.
88 L. T. Chen, W. Tam, S. H. Stevenson, G. R. Meredith, G. Rikken and S. R. Marder, *J. Phys. Chem.*, 1991, **95**, 10631–10643.
89 L. T. Chen, W. Tam, S. R. Marder, A. E. Stiegman, G. Rikken and C. W. Spangler, *J. Phys. Chem.*, 1991, **95**, 10643–10652.
90 *Molecular Nonlinear Optics: Materials, Physics and Devices*, ed. J. Zyss, Academic Press, Boston, 1994.
91 L. R. Dalton, A. W. Harper, R. Ghosn, W. H. Steier, M. Ziari, M. H. Fetterman, Y. Shi, R. V. Mustacich, A. K. Y. Jen and K. J. Shea, *Chem. Rev.*, 1995, **7**, 1060–1081.
92 Z. Cheng, L. R. Dalton, M.-C. Oh, Z. Hua and W. H. Steier, *Chem. Mater.*, 2001, **13**, 3043–3050.
93 A. J. Moore, A. Chesney, M. R. Bryce, A. S. Batsanov, J. F. Kelly, J. A. K. Howard, I. F. Perepichka, D. F. Perepichka, G. Meshulam, G. Berkovic, Z. Kotler, R. Mazor and V. Khodorkovsky, *Eur. J. Org. Chem.*, 2001, 2671–2687.
94 C. E. Powell and M. G. Humphrey, *Coord. Chem. Rev.*, 2004, **248**, 725–756.
95 J. L. Oudar and D. S. Chemla, *J. Chem. Phys.*, 1977, **66**, 2664–2668.
96 J. L. Oudar, *J. Chem. Phys.*, 1977, **67**, 446–457.